Journal of Translational Medicine

RESEARCH

Open Access

# Modulating tumor-associated macrophages through CSF1R inhibition: a potential therapeutic strategy for HNSCC

Kaiting Chen[1,2†], Xiaochen Li[1,2†], Shuyi Dong[2†], Yu Guo[1,2], Ziyin Luo[1,2], Shi-Min Zhuang[1,2], Jie Liu[1,2], Tianrun Liu[1,2,4*], Jing Liao[3*] and Weiping Wen[1,2,5*]

## Abstract

**Purpose** Tumor-associated macrophages (TAMs) are pivotal immune cells within the tumor microenvironment (TME), exhibiting dual roles across various cancer types. Depending on the context, TAMs can either suppress tumor progression and weaken drug sensitivity or facilitate tumor growth and drive therapeutic resistance. This study explores whether targeting TAMs can suppress the progression of head and neck squamous cell carcinoma (HNSCC) and improve the efficacy of chemotherapy.

**Methods** Bioinformatics analyses were performed to evaluate TAMs infiltration levels in HNSCC tumor tissues and examine their associations with patients' clinicopathological characteristics and prognosis. Flow cytometry was utilized to measure the expression of key macrophage markers and assess apoptosis following treatment with colony stimulating factor 1 receptor (CSF1R) inhibitors (BLZ945, PLX3397). Additionally, immunohistochemistry was employed to detect CD68 and CD8 expression. In vivo, the antitumor efficacy of CSF1R inhibitors was tested in mouse HNSCC tumor model, both as monotherapy and in combination with cisplatin, to evaluate potential synergistic effects.

**Results** Bioinformatic analysis identified TAMs as the predominant infiltrating immune cells in the TME of HNSCC, with significantly higher infiltration levels in tumor tissues compared to adjacent non-tumor tissues. High TAMs infiltration was associated with poorer overall survival (OS), disease-free survival (DFS), human papillomavirus (HPV) infection status, and advanced disease stages. The TAMs-related genes prediction model demonstrated high prognostic accuracy. CSF1R is primarily expressed in TAMs, where high CSF1R expression may suppress antigen binding and activation. In vitro experiments showed that CSF1R inhibitors induce TAMs apoptosis, enhance their phagocytic activity, and reduce CD206 expression and IL-10 secretion, thereby diminishing their immunosuppressive function. In vivo experiments revealed that while CSF1R inhibitors alone had limited efficacy in suppressing tumor growth, their combination with cisplatin significantly enhanced therapeutic efficacy, as evidenced by increased $CD8^+$ T cells infiltration within the TME.

†Kaiting Chen, Xiaochen Li and Shuyi Dong have contributed equally to this work.

*Correspondence:
Tianrun Liu
liutrun@mail.sysu.edu.cn
Jing Liao
liaojing@gzhmu.edu.cn
Weiping Wen
wenwp@mail.sysu.edu.cn
Full list of author information is available at the end of the article

**Conclusion** Targeting TAMs via CSF1R inhibition enhances the therapeutic efficacy of cisplatin in HNSCC. These findings suggest that CSF1R inhibitors hold promise as a component of combination therapy for HNSCC.

**Keywords** HNSCC, TAMs, CSF1R inhibitors, Cisplatin, Combination therapy

**Graphical abstract**

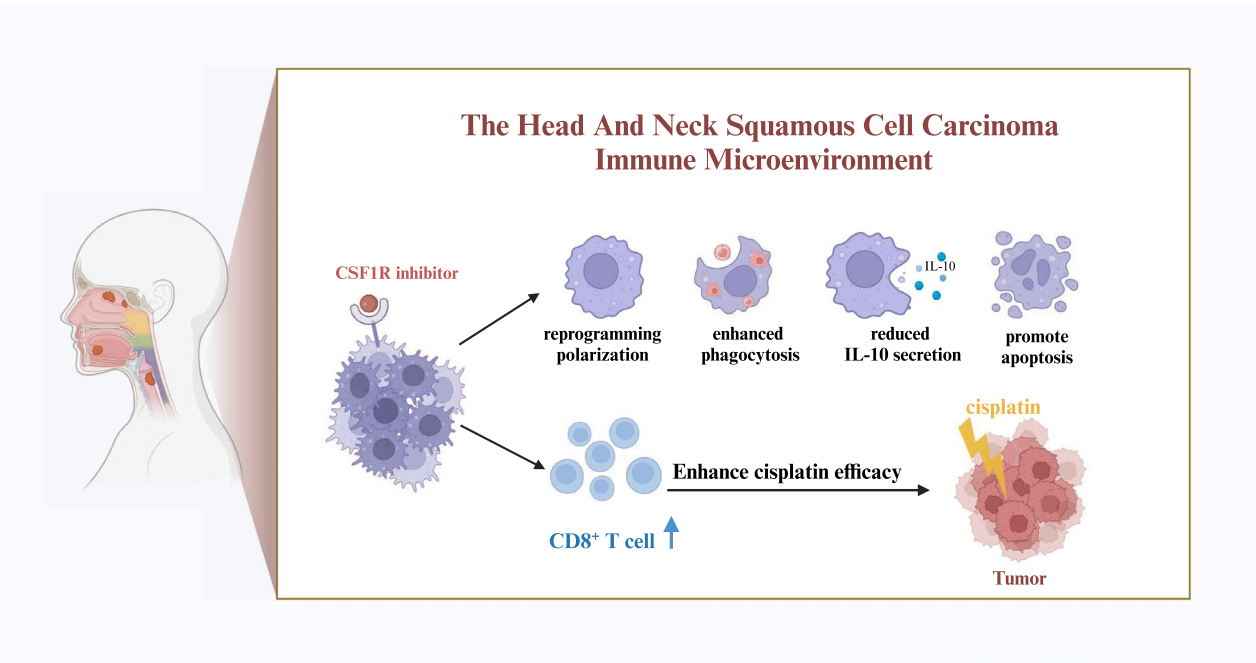


## Introduction

Head and neck squamous cell carcinoma (HNSCC) ranks as the seventh most common malignancy worldwide, with approximately 900,000 new cases and 450,000 deaths reported globally in 2022 [1]. The incidence of HNSCC continues to rise, and it is projected to increase by 30% by 2030 [2]. The etiology of HNSCC varies geographically: in Southeast Asia and Australia, smoking, betel nut chewing, and alcohol consumption are the primary risk factors, while in the United States and Western Europe, the growing incidence of oropharyngeal HNSCC is attributed to an increase in HPV infections [3–6]. Other risk factors include radiation exposure, wood dust, asbestos, salted foods, poor oral hygiene, and Epstein-Barr virus (EBV) infection [7, 8]. HNSCC is a highly heterogeneous malignancy, encompassing multiple anatomical sites and driven by diverse carcinogenic factors, each necessitating distinct therapeutic strategies. Treatment typically involves a multimodal strategy, incorporating surgery, radiation therapy, chemotherapy, immunotherapy, and targeted therapy. The choice of treatment depends on tumor location, stage, the patient's overall health, and molecular characteristics. Around 30–40% of HNSCC cases are detected at an early stage, where surgery or radiation alone can result in high cure rates [9]. However, early diagnostic tools remain inadequate, and more than 60% of patients are diagnosed at advanced or metastatic stages, often without evident premalignant lesions [10, 11]. According to the 2022 National Comprehensive Cancer Network (NCCN) guidelines, radiation therapy combined with cisplatin is the standard treatment for patients with locally advanced, unresectable HNSCC. For patients with recurrent or metastatic HNSCC, the EXTREME regimen (cetuximab + cisplatin or carboplatin + 5-FU) remains the first-line treatment [12]. Although initial responses are often favorable, most patients eventually develop resistance [13, 14]. Furthermore, conventional chemotherapy is non-selective and associated with significant side effects [15]. The introduction of epidermal growth factor receptor (EGFR) inhibitors marked a major advance in targeted therapy, yet many patients are either inherently resistant to these drugs or develop resistance during treatment [16]. In recent years, immune checkpoint inhibitors (PD-1 inhibitors), such as nivolumab and

pembrolizumab, have been approved for the treatment of recurrent or metastatic HNSCC that progresses during or after platinum-based chemotherapy. While some patients experience durable responses to PD-1 inhibitors, the overall efficacy remains limited, with only 17% of patients responding to monotherapy and a four-year survival rate below 30% [17]. Consequently, there is an urgent need for novel therapeutic approaches in HNSCC.

As research into the tumor microenvironment (TME) has advanced, the intricate interactions among cells and molecules within the TME have been increasingly recognized for their role in influencing tumor progression and treatment efficacy. TAMs, key regulatory factors within the TME, have emerged as significant players in cancer growth, invasion, metastasis, and treatment resistance [18]. Blood monocytes migrate to tumor sites in response to chemokines secreted by cancer cells and differentiate into either pro-inflammatory or anti-inflammatory phenotypes. In most solid tumors, TAMs tend to adopt an M2 phenotype, promoting tumor progression, while M1 TAMs exhibit anti-tumor functions [19]. TAMs can enhance anti-tumor immunity by phagocytosing cancer cells, but they can also facilitate immune evasion and tumor growth. TAMs heterogeneity is evident across different cancer types and stages of tumor progression [20]. High levels of TAMs infiltration are linked to poor prognosis in breast cancer [21], lung cancers [22], pancreatic cancers [23], melanoma [24] and Hodgkin's lymphoma [25]. While in colorectal cancer, TAMs infiltration is associated with better outcomes [26], although this relationship is reversed in colorectal liver metastases [27]. TAMs are not only linked to prognosis but also play a role in chemotherapy sensitivity [28]. Although much of the research on TAMs has focused on various solid tumors, studies specifically addressing the role of TAMs in HNSCC remain limited. However, emerging evidence suggests that TAMs play a crucial role in the progression and metastasis of HNSCC, and their involvement is gradually being recognized. Recent studies have shown that $SPP1^{+}$ TAMs are associated with lymph node metastasis and poor prognosis in HNSCC patients. $SPP1^{high}$ TAMs enhance tumor intravasation and metastasis in HNSCC through the secretion of SPP1, CCL18, and CXCL8 [29]. Furthermore, abnormal expression of ANXA3 has been shown to drive the reprogramming of TAMs toward M2 polarization, promoting an immunosuppressive microenvironment in Laryngeal Squamous Cell Carcinoma (LSCC). Additionally, ANXA3-enriched exosomes inhibit ferroptosis in LSCC cells via the ATF2-CHAC1 axis and promote lymphatic metastasis, thereby accelerating tumor progression [30]. Taken together, these findings highlight the pivotal role of TAMs in modulating the tumor microenvironment and enhancing metastatic potential in HNSCC. Given their high plasticity and heterogeneity, targeting TAMs through novel therapeutic strategies holds promise for improving patient survival and treatment outcomes in HNSCC.

Current strategies for targeting TAMs primarily focus on three approaches: depleting TAMs, reprogramming their polarization, and inhibiting their recruitment [19]. Among these, targeting CSF1R has garnered particular attention. By inhibiting CSF1R, not only can TAMs be depleted, but their recruitment and polarization can also be modulated [31]. CSF1R is a transmembrane tyrosine kinase receptor found on macrophages. Upon binding with its ligand CSF1, it induces receptor dimerization and tyrosine kinase-mediated phosphorylation, initiating intracellular signaling cascades that regulate macrophage survival, proliferation, differentiation, and migration [32–34]. Furthermore, targeting CSF1R in breast cancer has demonstrated potential synergistic effects when combined with chemotherapy or immunotherapy, and ongoing clinical trials are currently assessing this promising approach [35–39]. Although CSF1R inhibition has demonstrated the ability to regulate TAMs through multiple pathways in cancers such as pancreatic cancer [40], recent studies highlight that its efficacy may depend on the specific organ and tumor subtype [41]. While CSF1R inhibitors have shown promise in TAMs regulation, their role in HNSCC remains unclear. Therefore, this study aims to comprehensively investigate the relationship between TAMs infiltration, prognosis, and clinicopathological characteristics in HNSCC through bioinformatics analysis. Additionally, through in vivo and in vitro experiments, we elucidate the mechanisms by which CSF1R-targeted therapies regulate TAMs in HNSCC and evaluate the potential of CSF1R inhibitors as a therapeutic strategy for HNSCC.

## Methods

### Data source and preprocessing

We obtained mRNA expression data and clinical information from The Cancer Genome Atlas (TCGA) and the Gene Expression Omnibus (GEO) databases, specifically utilizing datasets GSE113282, GSE270220, and GSE107591. Immune cells infiltration in HNSCC was assessed using CIBERSORT, with TAMs defined as the sum of M0, M1, and M2 macrophages. Patients were categorized into high and low TAMs groups, as well as M0, M1 and M2 infiltration groups, CSF1R/CD68 expression groups, using the minimum $p$-value method determined via X-Tile software [42]. Kaplan–Meier survival analysis was performed to evaluate overall survival (OS) and disease-free survival (DFS), with statistical significance assessed using the log-rank test.

Further analysis of TAMs infiltration levels involved dividing patients into high and low infiltration groups based on the median TAMs infiltration level. The association between TAMs infiltration and clinical characteristics was evaluated using *t*-tests to determine statistical significance.

For single-cell analysis, we employed the Seurat v4.0 package to normalize, pool, and cluster the GSE188737 single-cell dataset. Classic markers were used to annotate broad cell populations, including epithelial cells (KRT7, KRT17), salivary cells (STATH), fibroblasts (COL1A2), endothelial cells (PECAM), and immune cells (PTPRC). Fibroblasts were further categorized into cancer-associated fibroblasts (CAFs; MMP2) and myofibroblasts (ACTA2), while immune cells were divided into T-cells (CD3E, NKG7), NK-cells (NKG7, XCL2), B-cells (CD79A), plasma cells (IGHG1), mast cells (TPSAB1), conventional dendritic cells (LAMP3), plasmacytoid dendritic cells (LILR4), and macrophages/monocytes (CD163) [43]. Following annotation, clustering was conducted to visualize CSF1R expression across various cell subclusters. TAMs subclusters were extracted, and based on CSF1R expression levels within TAMs, they were divided into CSF1R_High and CSF1R_Low groups using the median expression level as the cutoff. Differential gene expression analysis was performed between these groups, followed by functional enrichment analysis of differentially expressed genes using the clusterProfiler package in R. Gene symbols were converted to Entrez Gene IDs, and Gene Ontology (GO) enrichment analysis (Biological Process, BP) was conducted using Gene Set Enrichment Analysis (GSEA). The significance level for enrichment was set at $p < 0.05$, with results visualized through dot plots and GSEA enrichment curves.

#### Establishment of a prognostic model

To assess the prognostic value of TAMs-related genes, we selected 208 macrophage-related marker genes from the CellMarker database. We conducted univariate Cox regression analysis to evaluate the association between these genes and survival in the TCGA cohort, selecting those with $p$-value $< 0.05$ for further analysis. From this screening, 42 genes were identified as being significantly associated with survival and were used to develop a prognostic model using the LASSO Cox regression method. Risk scores were then calculated based on this model. 519 patients in the TCGA-HNSCC cohort were stratified into low-risk and high-risk subgroups according to their risk scores, using the minimum $p$-value method. LASSO regression analysis, along with univariate and multivariate Cox regression analyses, was employed to validate the model. Kaplan–Meier analysis was performed to compare OS between the two subgroups. The model's sensitivity and specificity were further assessed using time-dependent receiver operating characteristic (ROC) analysis.

#### Cell culture and drug

We obtained the murine oral squamous cell carcinoma (OSCC) cell line MTCQ1, which is derived from HNSCC, from the Bioresource Collection and Research Center (BCRC). Additionally, we acquired the murine fibroblast cell line L929 from the American Type Culture Collection (ATCC). All cell lines were tested for mycoplasma contamination using a single-step polymerase chain reaction (PCR) method. The cells were cultured in high-glucose DMEM (Procell) medium supplemented with 10% fetal bovine serum (FBS), 100 U/mL penicillin (Beyotime), and 100 μg/mL streptomycin (Beyotime) in a humidified incubator at 37 °C with 5% $CO_2$.

We purchased anti-mouse CSF1R (clone: AFS98) from BioXcell and CSF1R small-molecule inhibitors Pexidartinib (PLX-3397, HY-16749A) and Sotuletinib (BLZ945, HY-12768A) from MCE for use in mouse tumor treatments and in vitro cell experiments.

#### BMDMs generation and in vitro stimulation

Euthanize 6–8-week-old mice, carefully opening the abdominal skin to expose the femur and tibia. Immerse the bones in 75% ethanol for 30 s, followed by a rinse with PBS. Trim the ends of the bones and flush the marrow cavity with serum-free medium containing antibiotics until the bones appear white. Filter the bone marrow suspension through a 75 μm cell strainer into a centrifuge tube, wash twice with PBS, and centrifuge at 1500 rpm for 5 min. Discard the supernatant, then add 2 ml of ACK lysis buffer to lyse red blood cells for 1–1.5 min, terminating the reaction by adding PBS. Centrifuge at 600 g for 5 min, discard the supernatant, and repeat the PBS wash. Resuspend the cells in complete medium supplemented with 30% L929-conditioned medium and seed them at a density of $1 \times 10^7$ cells per 10 cm dish. Incubate at 37 °C with 5% $CO_2$. On days 3 and 5, perform a half-medium change. On day 7, discard the supernatant, wash with PBS, and add a 1:1 mixture of MTCQ1 tumor cell-conditioned medium (cultured for 48–72 h, supplemented with 10% FBS) and complete medium to induce TAMs. Add 20 ng/ml LPS to induce classical M1 macrophages and 20 ng/ml IL-4 to induce M2 macrophages. After 40 h, collect the cells and perform flow cytometry to characterize the following groups: NTC (30% L929-conditioned medium), LPS-induced classical M1 macrophages, IL-4-induced M2 macrophages, and tumor-conditioned medium-induced TAMs, using the following antibodies: CD11b (Biolegend, Cat: 101208), F4/80 (Biolegend, Cat: 123114), CD11c (Biolegend, Cat:

117339), MHC I (Biolegend, Cat: 114605), MHC II (Biolegend, Cat: 107608), CD80 (Biolegend, Cat: 104706), CD86 (Biolegend, Cat: 105013), CD163 (Invitrogen, Cat: 12–163-82), CD206 (Biolegend, Cat: 141708), and PD-L1 (Biolegend, Cat: 124321).

#### Phagocytosis

To assess the impact of CSF1R small molecule inhibitors on the phagocytic capacity of TAMs, MTCQ1 tumor cells were first pre-incubated with 5 μM carboxyfluorescein succinimidyl ester (CFSE) at 37 °C for 10 min. The reaction was halted by adding DMEM containing 10% FBS. After thorough washing with PBS twice, the cells were incubated with 100 μg/mL mitomycin C at 37 °C for 10 min. The cells were then washed twice with DMEM containing 10% FBS, harvested, and co-cultured with TAMs at a 1:1 ratio ($1\times10^6$ cells/well) in a 6-well plate for 2 h. Afterward, the supernatant was discarded, and the wells were washed twice with PBS to remove non-phagocytosed tumor cells. Phagocytic activity was evaluated using a fluorescence microscope (Olympus) by calculating the percentage of macrophages containing CFSE-labeled green fluorescence.

#### Flow cytometry

TAMs treated with DMSO, PLX3397, or BLZ945 for 48 h were stained to detect the expression of relevant mouse proteins using the following antibodies: anti-mouse CD206 (Biolegend, Cat: 41,707), anti-mouse CD86 (Biolegend, Cat: 105,023), and Anti-Mouse MHC Class II V5-Tag-Alexa Fluor 647 (ONBO Biosciences, Cat: GTX80040). Additionally, apoptosis was assessed using the Annexin V-FITC/PI apoptosis kit (liankebio). The stained cells were analyzed using a CytoFLEX S flow cytometer (Beckman Coulter), and data analysis was performed with FlowJo V10.8 software (TreeStar).

#### Measurement of IL-10 secretion by ELISA

Supernatants from TAMs treated with DMSO, PLX3397, or BLZ945 for 48 h were collected and stored at −80 °C. A protease inhibitor cocktail (Invitrogen) was added in accordance with the manufacturer's instructions. IL-10 levels were quantified using the Mouse IL-10 Uncoated ELISA Kit (Invitrogen), following the provided protocol.

#### Mice and tumor model

We obtained SPF-grade 6–8 week-old male C57BL/6 mice from Guangdong Medical Laboratory Animal Center. All animal experiments were approved by the Institutional Animal Care and Use Committee (IACUC) of the Sixth Affiliated Hospital of Sun Yat-sen University, with approval numbers IACUC-2023101306 and IACUC-2022010601.

In brief, $3\times10^6$ MTCQ1 tumor cells were subcutaneously (s.c.) implanted into the right flanks of the mice [44]. Tumor volume was measured along three orthogonal axes (a, b, and c) and calculated using the formula: Tumor Volume = abc/2.

Treatment with the anti-CSF1R antibody (10 mg/kg, i.p.), PLX3397 (60 mg/kg, p.o.), and BLZ945 (60 mg/kg, p.o.) began on the day of implantation and was administered every 3 days until the end of the experiment. When the tumor volume reached approximately 100 cubic millimeters, cisplatin was administered intraperitoneally (i.p.) at a dose of 10 mg/kg once a week.

#### Immunohistochemistry and image analysis

Tumor samples and paired adjacent non-tumor tissues were collected from 12 HNSCC patients at the Sixth Affiliated Hospital of Sun Yat-sen University between January 2020 and December 2023. The study received approval from the Ethics Committee (approval numbers 2020ZSLYEC-303 and 2021ZSLYEC-270), and informed consent was obtained from all patients or their legal guardians. Immunohistochemistry (IHC) was performed on these samples using anti-CD68 and CD163 antibodies. Additionally, subcutaneous tumor samples from MTCQ1 mice were collected for CD8, F4/80, CD163, and iNOS IHC analysis.

Tissue sections of 4 μm were placed in an oven at 60 ℃ for 20 min. Deparaffinization was performed using two xylene treatments (10 min each), followed by rehydration through a graded ethanol series (100%, 95%, 85%, and 75%, 3 min each) and washing in $ddH_2O$. Antigen retrieval was conducted by boiling the sections in Tris–HCl buffer (pH 9.2) in a pressure cooker for 10 min. After cooling, sections were incubated with endogenous peroxidase blocking solution (Beyotime, Cat: P0100B) at room temperature for 10 min. Blocking was then done with 5% bovine serum albumin (BSA) for 30 min at room temperature. Sections were incubated overnight at 4 °C with anti-CD68 antibody (Sino Biological, Cat: 11,192-T56, 1:500), anti-CD163 antibody(abclonal, Cat: A25206, 1:500), anti-CD8α antibody (Abcam, Cat: ab217344, 1:500), anti-F4/80 antibody (CST, Cat: 700,765, 1:500), anti-CD163 antibody (Abcam, Cat: ab182422, 1:500), anti-iNOS antibody (Abcam, Cat: ab15323, 1:100), followed by a 30-min incubation at room temperature with horseradish peroxidase-conjugated anti-rabbit antibody (Beyotime, Cat: A0208, 1:50). Staining was visualized using a DAB detection kit (ZSGB-BIO, Cat: ZLI-9017).

Slides were scanned at ×40 magnification using the SQS-1000 slide scanner (Shenzhen Shengqiang Technology Co., Ltd., China). Digital image analysis was performed using ImageJ software (version 1.54d). Two independent researchers evaluated the tumor samples,

examining five distinct areas per section. The histological scores for CD68, F4/80, CD163 (mouse), and iNOS were determined by multiplying the proportion score by the intensity score. Additionally, the average optical density (AOD) was used to quantify the proportion of CD8-positive cells and CD163 (human), with the final results reported as the mean of these measurements.

### Statistical analyses

Data were analyzed using Prism 8.0.2 software (GraphPad) and are presented as mean ± SEM. The significance of differences between two groups was assessed using the Wilcoxon rank-sum test, paired Student's *t*-test, or unpaired Student's t-test, as appropriate. Differences among multiple groups were evaluated using ANOVA. Overall survival (OS) was defined as the time from surgery to death from any cause. Disease-free survival (DFS) was defined as the time following treatment during which patients remained free from cancer recurrence or progression. Survival rates were estimated using the Kaplan–Meier method, with comparisons made using the log-rank test. All *p*-values were two-sided, with $p < 0.05$ considered statistically significant.

## Results

### TAMs infiltration and prognostic significance in HNSCC

In the TCGA and GSE113282 datasets, TAMs were identified as the predominant component of immune infiltration within HNSCC tumors (Fig. 1a, b). Kaplan–Meier survival analysis of the TCGA cohort demonstrated that high TAMs infiltration was significantly associated with poorer overall survival (OS) ($p = 0.001$, HR = 1.581) (Fig. 1c). Further stratification of TAMs into M0, M1, and M2 subtypes revealed that high infiltration of M0 ($p = 0.006$, HR = 1.673) and M2 ($p = 0.037$, HR = 1.426) macrophages was significantly correlated with worse patient survival, whereas M1 ($p = 0.514$, HR = 1.157) macrophage infiltration did not show a significant association with survival (Supplementary Fig. 1). Similarly, in the GSE270220 dataset, elevated TAMs infiltration correlated with lower disease-free survival (DFS) ($p = 0.006$, HR = 5.056) (Fig. 1d). Paired analysis of tumor versus non-tumor tissues in the TCGA and GSE107591 datasets demonstrated a significant increase in TAMs infiltration within tumor tissues (Fig. 1e, f). Immunohistochemical analysis further confirmed this finding, showing markedly higher CD68 and CD163 expression in HNSCC tissues compared to adjacent non-tumor tissues (Fig. 1g). Clinical feature analysis of the TCGA-HNSCC cohort indicated that high TAMs infiltration was significantly associated with HPV status ($p < 0.001$), T stage ($p < 0.001$), N stage ($p = 0.013$), overall TNM stage ($p < 0.001$), and clinical grade ($p = 0.029$) (Table 1). These results demonstrate that TAMs play an important role in the immune microenvironment of HNSCC. High levels of TAMs infiltration are associated with poorer survival outcomes and more advanced disease stages. However, while these findings underscore the potential of TAMs as key components of the tumor microenvironment, further research is required to validate their role as reliable biomarkers or therapeutic targets.

### Construction of the risk signature

Univariate Cox analysis in the TCGA cohort identified 42 genes significantly associated with OS, which were further refined using LASSO regression to construct a risk signature (Fig. 2a–c). This risk model effectively stratified patients into high- and low-risk groups, with the high-risk group showing significantly poorer OS ($p < 0.001$) (Fig. 2d). The ROC curve analysis demonstrated that the predictive model had good accuracy (AUC = 0.70 for 1-year, 0.674 for 2-year, and 0.69 for 3-year survival) (Fig. 2e). Both univariate and multivariate Cox regression analyses confirmed that TAMs infiltration was an independent prognostic factor for OS in HNSCC (Fig. 2f).

### CSF1R expression and its impact on immune function and prognosis

UMAP analysis of scRNAseq data from seven HNSCC samples in the GSE188737 dataset showed that *CSF1R* expression was predominantly localized to TAMs, with a strong correlation to macrophage markers (Fig. 3a, b). In the TCGA dataset, *CSF1R* gene expression had the highest Pearson correlation with macrophages. Our analysis revealed a significant positive correlation between *CSF1R* expression and TAMs infiltration ($p < 0.001$, R = 0.734) (Fig. 3c, d). Additionally, we assessed the relationship between *CSF1R* expression and M2 TAMs infiltration and found a positive correlation ($p < 0.001$, R = 0.338) (Fig. 3e). Moreover, *CSF1R* expression was significantly higher in tumor tissues compared to adjacent non-tumor tissues ($p < 0.05$) (Fig. 3f). Kaplan–Meier analysis in the GSE270220 dataset indicated that high *CSF1R* / *CD68* expression was significantly associated with poorer DFS ($p = 0.025$, HR = 2.580) (Fig. 3g). GO enrichment analysis of TAMs at the single-cell level suggested that TAMs with low *CSF1R* expression were involved in antigen binding and activation functions, implying that CSF1R inhibition may enhance anti-tumor immunity (Fig. 3h). These results suggest that high *CSF1R* expression in HNSCC is closely associated with the functional regulation of tumor-associated macrophages, and that CSF1R inhibition may improve patient prognosis by enhancing anti-tumor immune responses.

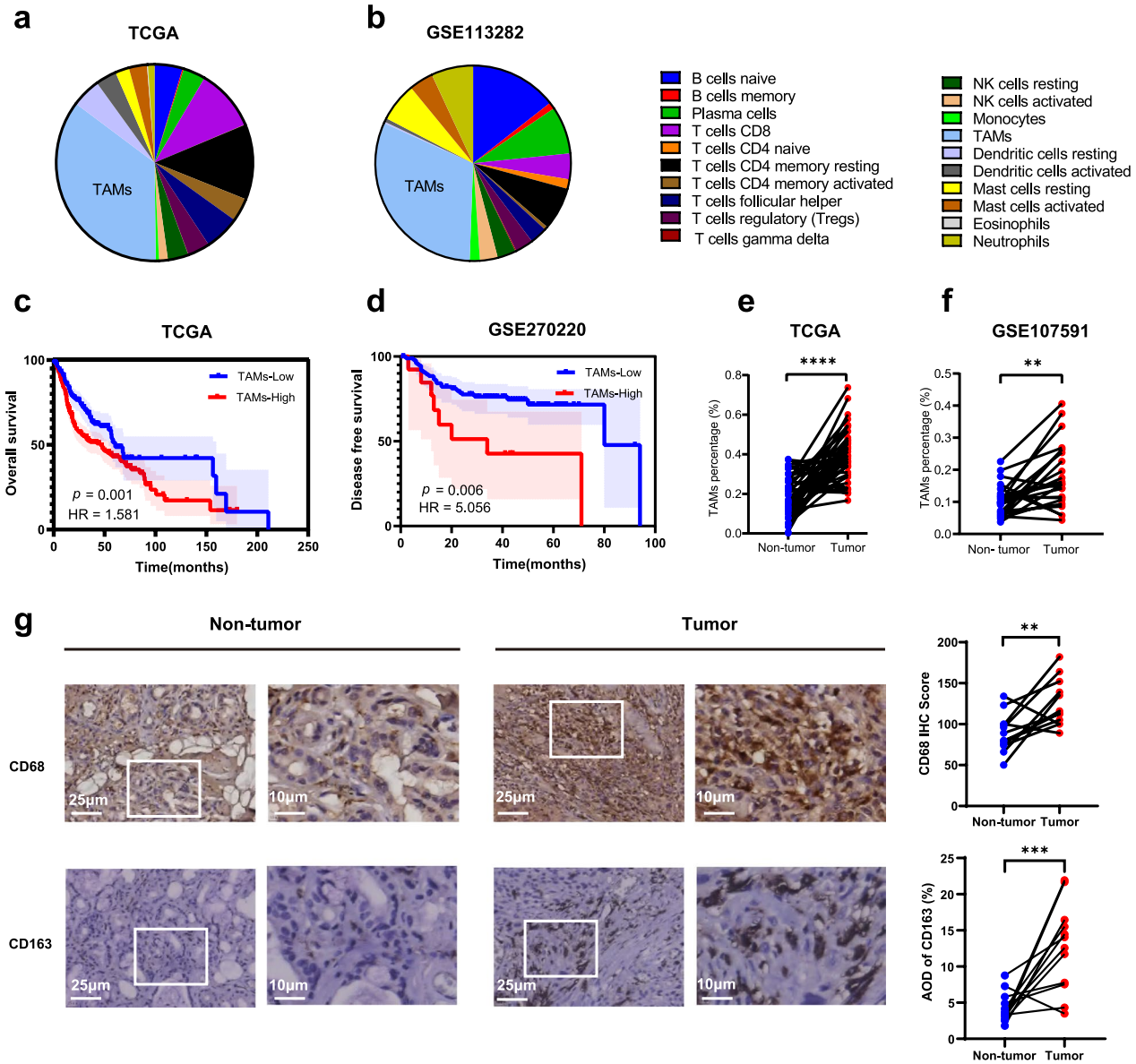


**Fig. 1** The impact of TAMs infiltration on HNSCC incidence and prognosis. **a** Immune infiltration in HNSCC was assessed using CIBERSORT analysis of the TCGA **a** and GSE113282 **b** datasets. TAMs are defined as the sum of M0, M1, and M2 macrophages (TCGA, n = 519; GSE113282, n = 100). **c** Patients in the TCGA-HNSCC cohort were divided into high and low TAMs infiltration groups based on the minimum *p*-value approach. Kaplan–Meier survival curves were calculated and analyzed using the log-rank test ($p = 0.012$), n = 519. **d** Patients in the GSE270220 dataset were similarly categorized, and disease-free survival was analyzed with Kaplan–Meier curves and the log-rank test ($p = 0.006$), n = 109. **e**–**f** TAMs infiltration in paired adjacent non-tumor and tumor tissues from 43 HNSCC patients in TCGA **e** and 23 patients in GSE107591 **f** was assessed using paired *t*-tests (TCGA, n = 43; GSE107591, n = 23). **g** Differential expression of CD68 in HNSCC and CD163 non-tumor tissues and tumor tissues from twelve patients at The Sixth Affiliated Hospital of Sun Yat-sen University was analyzed by IHC and paired *t*-tests. Scale bars = 25 μm / 10 μm, n = 12. **, $p < 0.01$; ****, $p < 0.0001$

**Effects of CSF1R inhibitors on TAMs function and survival**

Pexidartinib (PLX3397) and Sotuletinib (BLZ945) are two promising CSF1R inhibitors. PLX3397 primarily targets CSF1R and also inhibits KIT and FLT3 [45]. It has gained considerable attention for its ability to suppress the proliferation of TAMs, which are key players in tumor progression and immune evasion [46]. Recently, PLX3397 was approved by the U.S. Food and Drug Administration (FDA) for the treatment of tenosynovial giant cell tumors (TGCT) [47, 48]. Similarly, Sotuletinib (BLZ945) specifically targets CSF1R, though it differs structurally from PLX3397. Despite these differences, both inhibitors act by

**Table 1** TCGA-HNSCC cohort clinical characteristics by high/low TAMs infiltration using median cutoff

| | High TAMs | Low TAMs | *p* |
|---|---|---|---|
| n | 260 | 259 | |
| Age (years) = > 60 (%) | 132 (50.8) | 130 (50.2) | 0.965 |
| Sex = Male (%) | 189 (72.7) | 194 (74.9) | 0.636 |
| Race (%) | | | 0.977 |
| American Indian or Alaska Native | 1 (0.4) | 1 (0.4) | |
| Asian | 6 (2.3) | 5 (1.9) | |
| Black or African American | 25 (9.6) | 23 (8.9) | |
| White | 222 (85.4) | 222 (85.7) | |
| NA | 6 (2.3) | 8 (3.1) | |
| HPV_state (%) | | | **< 0.001** |
| HNSC_HPV- | 226 (86.9) | 189 (73.0) | |
| HNSC_HPV + | 17 (6.5) | 55 (21.2) | |
| NA | 17 (6.5) | 15 (5.8) | |
| T_stage (%) | | | **< 0.001** |
| Low T_stage | 87 (33.5) | 98 (37.8) | |
| High T_stage | 155 (59.6) | 117 (45.2) | |
| NA | 18 (6.9) | 44 (17.0) | |
| N_stage (%) | | | **0.013** |
| Node negative | 86 (33.1) | 90 (34.7) | |
| Node Positive | 136 (52.3) | 108 (41.7) | |
| NA | 38 (14.6) | 61 (23.6) | |
| Stage (%) | | | **< 0.001** |
| I-II | 46 (17.7) | 54 (20.8) | |
| III-IV | 193 (74.2) | 153 (59.8) | |
| NA | 21 (8.1) | 50 (19.3) | |
| Grade (%) | | | **0.029** |
| Low Grade | 194 (74.6) | 171 (66.0) | |
| High Grade | 60 (23.1) | 72 (27.8) | |
| NA | 6 (2.3) | 16 (6.2) | |
| Radiation_Therapy (%) | | | 0.772 |
| No | 79 (30.4) | 77 (29.7) | |
| Yes | 145 (55.8) | 151 (58.3) | |
| NA | 36 (13.8) | 31 (12.0) | |

The bold values indicate statistically significant results with $p < 0.05$

blocking CSF1R signaling, which reduces TAMs populations and inhibits their pro-tumor functions [49]. Both compounds are being investigated for their potential to modulate the tumor microenvironment and serve as therapeutic agents across various cancers. Currently, PLX3397 and BLZ945 are in Phase I and Phase II clinical trials for the treatment of advanced solid tumors (NCT02734433, NCT02829723). Based on their promising mechanisms, we selected these two CSF1R small-molecule inhibitors for investigation in our study.

Using specific markers (CD11b, F4/80, CD11c, MHC I, MHC II, CD80, CD86, CD163, CD206, PD-L1), we confirmed that TAMs induced by MTCQ1 tumor cell supernatant (TCS) were predominantly macrophages, not dendritic cells (DCs). Compared to classical LPS-induced M1 macrophages and IL-4-induced M2 macrophages, TAMs stimulated by MTCQ1 TCS exhibited a similar expression profile for MHC I, CD80, CD163, CD206, and PD-L1 to M2 cells, while their MHC II and CD86 expression was more similar to that of M0 and M1 macrophages. Overall, TAMs induced by MTCQ1 TCS displayed an M2-like phenotype (Supplementary Fig. 2). In vitro studies demonstrated that treatment of TAMs with CSF1R inhibitors (PLX3397, BLZ945) led to significant morphological changes and enhanced their phagocytic activity (Fig. 4a, b). Initial observations suggested that CSF1R inhibitors might inhibit TAMs polarization. To gain deeper insights into the expression of M2 markers and M1 markers on TAMs, Flow cytometry analysis revealed that both inhibitors reduced the expression of the M2 typical marker CD206. PLX3397 notably increased CD86 expression in TAMs, while BLZ945 only slightly upregulated CD86. However, PLX3397 decreased MHC II expression, whereas BLZ945 slightly increased MHC II expression (Fig. 4c). Furthermore, CSF1R inhibitors significantly reduced IL-10 secretion and increased TAMs apoptosis (Fig. 4d, e). Collectively, these findings suggested that CSF1R inhibitors shift TAMs towards the M1 macrophage phenotype, suppressed M2 macrophage differentiation, enhance macrophage-mediated phagocytosis of tumor cells, and reduced TAMs survival and immunosuppressive functions.

### Efficacy of CSF1R inhibitors alone and in combination with cisplatin in vivo

To further assess the in vivo efficacy of CSF1R inhibition, a subcutaneous HNSCC model was established by injecting cancer cells directly into mice. The results showed that treatment with PLX3397 significantly inhibited tumor growth; however, neither α-CSF1R antibody nor BLZ945 alone effectively controlled tumor progression (Fig. 5a–c). When combined with cisplatin, all three CSF1R-targeted therapies led to a marked reduction in tumor growth and

(See figure on next page.)

**Fig. 2** Construction of a risk signature in the TCGA cohort. **a** Univariate Cox analysis identified 42 genes associated with survival ($p < 0.05$). **b** LASSO regression was performed on these 42 OS-related genes. **c** Variation of each coefficient under different lambda values is shown, with the x-axis representing the logarithm of lambda and the y-axis representing the coefficient. **d** Based on associated risk factors, patients were categorized into high and low TAMs infiltration groups. Kaplan–Meier survival curves were analyzed ($p < 0.001$), n = 519. **e** ROC curve AUCs for 1-, 3-, and 5-year OS prediction in the TCGA-HNSCC cohort. **f** Univariate (left) and multivariate (right) Cox regression analyses for overall survival

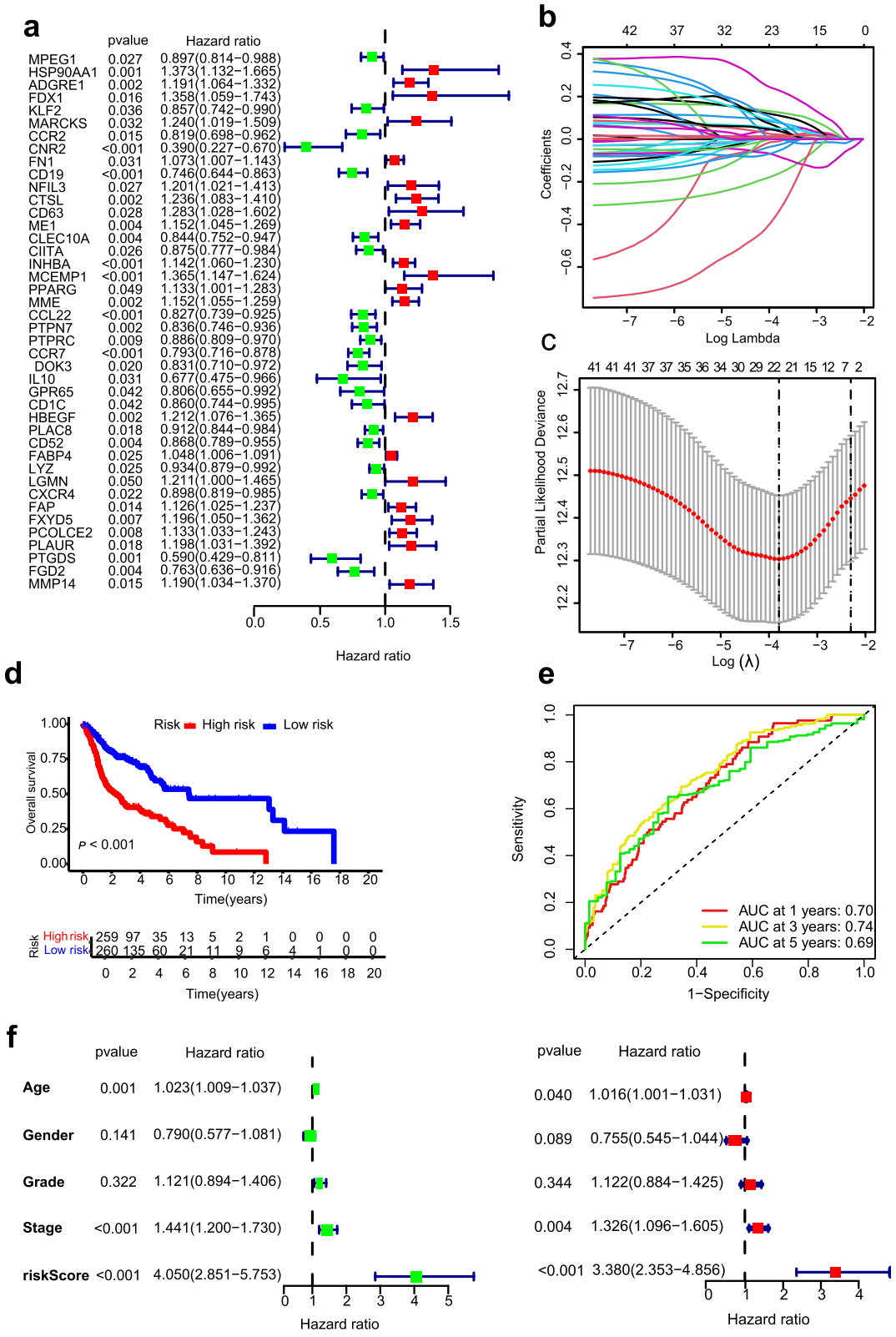


**Fig. 2** (See legend on previous page.)

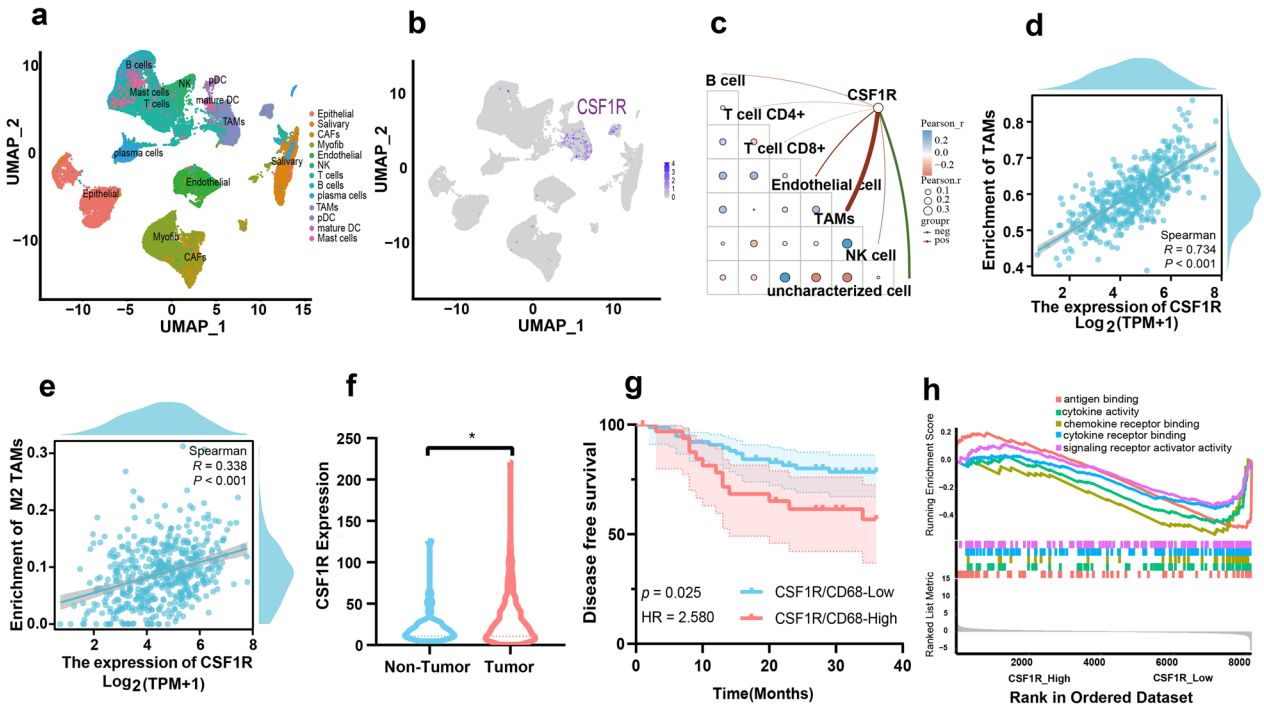


**Fig. 3** Impact of CSF1R expression on survival prognosis and immune function. **a** UMAP plot of single cells from twelve patient-derived primary HNSCC samples, n = 7. **b** UMAP of *CSF1R* expression in tumor-specific clusters. **c** Pearson correlation between *CSF1R* expression and various cell types in the TCGA-HNSCC. **d** Spearman correlation analysis between *CSF1R* expression and TAMs infiltration levels in the TCGA-HNSCC cohort. **e** Spearman correlation analysis between *CSF1R* expression and M2 TAMs infiltration levels in the TCGA-HNSCC cohort. **f** Expression levels of *CSF1R* in tumor and adjacent non-tumor tissues from the TCGA-HNSCC database. **g** Patients in the GSE220270 dataset were divided into low and high *CSF1R/CD68* groups based on the minimum *p*-value statistics. Disease-free survival was analyzed using Kaplan–Meier curves and the log-rank test ($p = 0.025$), n = 109. **h** GO enrichment analysis of low CSF1R TAMs involved in antigen binding and activation functions in the GSE188737 single-cell dataset

(See figure on next page.)

**Fig. 4** Effects of CSF1R inhibitors on TAMs functions and survival. **a** Representative images of TAMs morphology after treatment with PBS (no treatment control, NTC), PLX3397, or BLZ945. Scale bar = 50 μm. **b** Phagocytosis was assessed using CFSE-labeled MTCQ1 tumor cells and confocal microscopy, comparing PLX3397, BLZ945, and PBS (no treatment control, NTC), n = 6. **c** TAMs treated with PLX3397 and BLZ945 for 48 h were analyzed by flow cytometry for CD206, CD86, and MHC II expression. **d** IL-10 concentration in supernatants of TAMs treated with PLX3397 and BLZ945 was measured by ELISA, n = 4. **e** Flow cytometry analysis of TAMs for apoptotic cell percentages after 48 h of treatment with PLX3397 and BLZ945, n = 4. Each experiment was conducted at least twice with consistent results, and representative data from two independent experiments are presented. Each experimental group includes at least three independent samples. *, $p < 0.05$; **, $p < 0.01$; ***, $p < 0.001$; ****, $p < 0.0001$

weight compared to the control or monotherapy groups (Fig. 5d–f). Immunohistochemical analysis indicated an increase in $CD8^+$ T cells infiltration in the tumors of the combination treatment group, suggesting an enhanced antitumor immune response. We hypothesize that the increased infiltration of $CD8^+$ T cells may contribute to the enhanced efficacy of cisplatin when combined with CSF1R inhibitors (Fig. 5g, h). To explore this further, we performed immunohistochemical (IHC) analysis to assess TAMs (F4/80), M1 (iNOS), and M2 (CD163) macrophages in subcutaneous tumor tissues. Treatment with CSF1R inhibitors significantly decreased the expression of F4/80 and CD163, indicating reduced infiltration of TAMs and M2 macrophages. Additionally, α-CSF1R monoclonal antibody treatment also reduced iNOS expression, suggesting a decrease in M1 infiltration. However, no significant changes in M1 markers were observed with small molecule inhibitors (PLX3397 and BLZ945) (Supplementary Fig. 3). Furthermore, spearman correlation analysis suggested that high TAMs infiltration is associated with lower $CD8^+$ T cells infiltration in the TCGA-HNSCC cohort ($p < 0.001$, $R = -0.478$) (Fig. 5i). CSF1R inhibitors alone showed limited

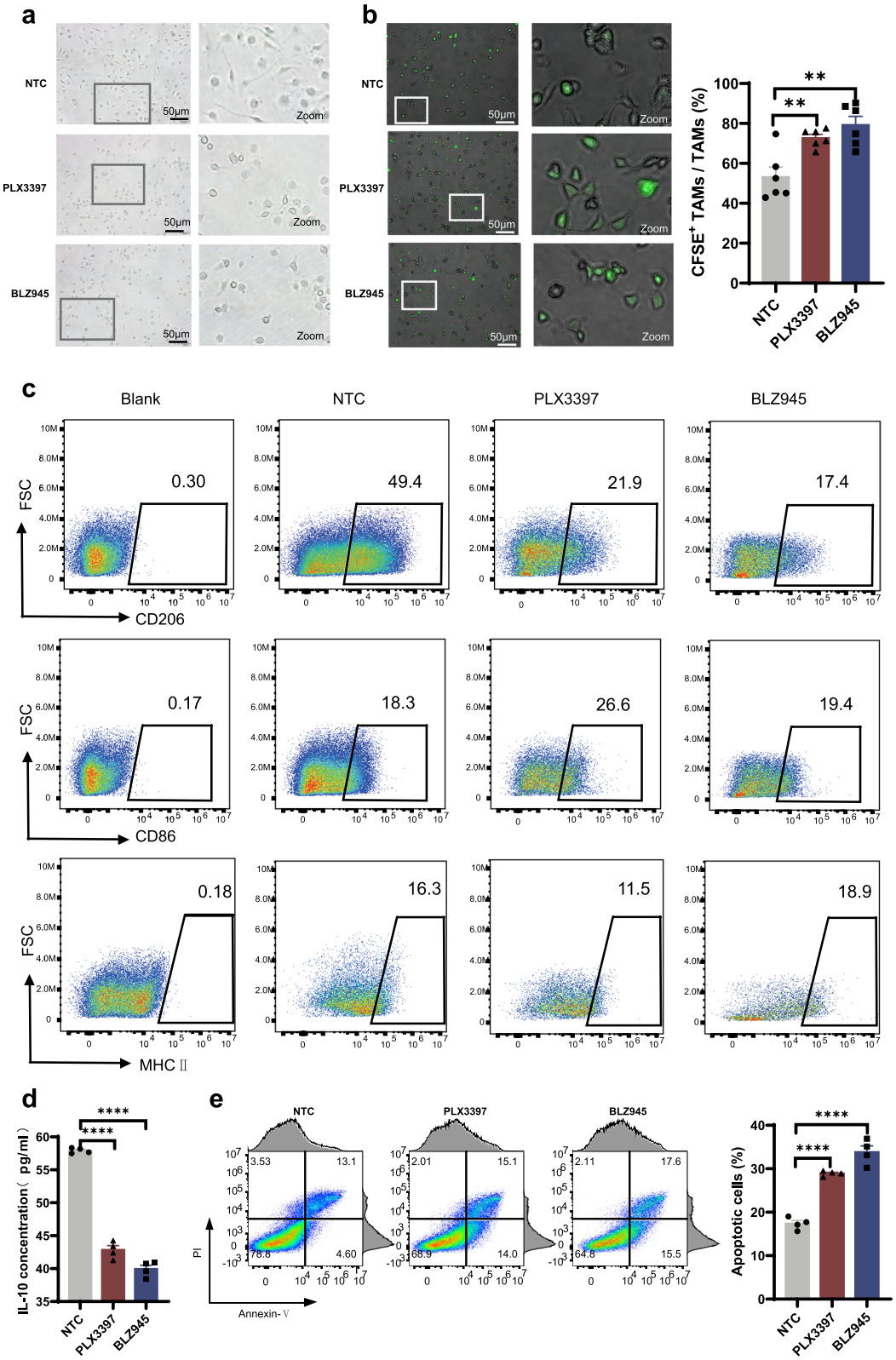


**Fig. 4** (See legend on previous page.)

effectiveness in suppressing tumor growth; however, when combined with cisplatin, they significantly enhanced therapeutic efficacy, possibly due to the increased infiltration of $CD8^+$ T cells within the tumor microenvironment. These results suggest that CSF1R inhibitors reduce TAMs and M2 infiltration, which may enhance anti-tumor immunity, potentially by promoting $CD8^+$ T cells infiltration. Further experiments are needed to confirm this hypothesis.

## Discussion

TAMs are abundant in the TME and play critical roles in tumor progression, metastasis, and poor prognosis, as observed in HNSCC. Through bioinformatics analysis of multiple datasets, we found that high infiltration of TAMs or M2 TAMs is significantly associated with poorer overall survival (OS), disease-free survival (DFS), HPV infection status, and advanced clinical staging and grading in HNSCC patients. Consistent with previous reports, semi-quantitative immunohistochemistry studies have shown that high infiltration of CD68-positive macrophages and elevated CD163 expression are correlated with worse OS in oral OSCC patients [50]. Additionally, high CD163 expression in primary HNSCC tumors is associated with poor survival outcomes, particularly in HPV-negative patients [51]. The density of $CD163^+$ M2-TAMs also correlates with poor prognosis, lymph node metastasis, and advanced clinical stage [52]. Our TAMs-related gene prediction model demonstrated strong prognostic accuracy, further supporting the development of TAMs-targeted therapies.

CSF1R inhibitors, as key therapeutic agents targeting the CSF1R signaling pathway, have emerged as promising treatments for modulating TAMs function. Currently, targeted therapies against CSF1R are being actively explored, both as standalone treatments and in combination with other therapies. In a murine model of pre-neoplastic glioblastoma, CSF1R inhibitors significantly improved survival and suppressed tumor growth. Moreover, CSF1R inhibition markedly slowed the intracranial growth of patient-derived glioblastoma xenografts [53]. These trials demonstrated a reduction in tumor burden and effective disease control in treated patients including glioblastoma (NCT01349036), pancreatic cancer (NCT02777710), and breast cancer (NCT01525602). However, in various subtypes of breast cancer, although TAMs can be reduced by CSF1R inhibitors, the overall effectiveness in controlling certain breast cancer subtypes remains limited [54]. Furthermore, PLX3397 reduced circulating $CD14^{dim}/CD16^+$ monocytes in recurrent glioblastoma [55], but did not significantly extend OS in a Phase II trial. (NCT01349036), raising concerns about its clinical efficacy. In our study, only PLX3397 slowed tumor growth in the HNSCC mouse model, while other inhibitors had limited effects. Some studies have shown that targeting macrophages can significantly inhibit tumor progression, while others have not demonstrated substantial efficacy, leading to ongoing debates about the validity and applicability of macrophage-targeted therapies. Although its effectiveness as a monotherapy is limited, combining CSF1R inhibitors with other treatments enhances therapeutic outcomes. For instance, combining CSF1R inhibitors with paclitaxel improved survival in tumor-bearing mice by slowing primary tumor progression and reducing lung metastasis [36]. In rectal cancer, the combination of PLX3397 with anti-PD-1 mAb and anti-CTLA-4 mAb demonstrates effective synergistic effects [38]. Blockade of CSF1R signaling inhibits tumor-infiltrating myeloid cells and enhances the efficacy of radiotherapy in prostate cancer [56]. Likewise, our in vivo experiments also demonstrated that combining CSF1R inhibitors with cisplatin significantly enhanced anti-tumor efficacy, further supporting the potential of combination therapies.

CSF1R inhibitors modulate the TME by depleting TAMs, particularly M2 macrophages, and promoting their reprogramming toward the M1 phenotype, thus enhancing anti-tumor immunity. In vitro, CSF1R inhibitors reduced CD206 expression and increased CD86 and MHC II levels, driving TAMs toward M1 polarization. In vivo, they similarly reduced TAM and M2 macrophage infiltration. We hypothesize that CSF1R inhibitors primarily function by depleting

(See figure on next page.)

**Fig. 5** Efficacy of CSF1R inhibitors alone and in combination with cisplatin in vivo. **a**-**c** WT C57 mice were injected with MTCQ1 cells and treated with 60 mg/kg PLX3397 (**a**), 60 mg/kg BLZ945 (**b**), or PBS (no treatment control, NTC) orally every 3 days. Additionally, 10 mg/kg anti-CSF1R (**c**) or NTC was administered intraperitoneally, n = 4 to 6. **d**-**h** Mice were treated similarly, with the addition of 10 mg/kg cisplatin or NTC administered intraperitoneally every 7 days, n = 4 to 5. **d** Tumor growth curves for each treatment group. Line graphs show mean ± SEM. **e** Tumor weights for each group. **f** Representative images of tumor morphology on day 33 for each group. **g** IHC staining for CD8 in MTCQ1 mouse HNSCC tissue. Scale bars = 25 μm / 10 μm. **h** Quantitative analysis of CD8-positive T cells in randomly selected regions. *p*-values were calculated by Student's *t*-test, n = 12 to 16. *, $p < 0.05$; **, $p < 0.01$; ***, $p < 0.001$; ****, $p < 0.0001$. **i** Spearman correlation analysis was conducted to evaluate the relationship between TAMs infiltration levels and $CD8^+$ T cells infiltration in the TCGA-HNSCC cohort ($p < 0.001$, R = −0.478). Experiments a-c show representative results from two independent repeats of three separate experiments, with each group containing at least four mice. Experiments d-f show results from the same experiment (representative results from two independent repeats), with each group also containing at least four mice

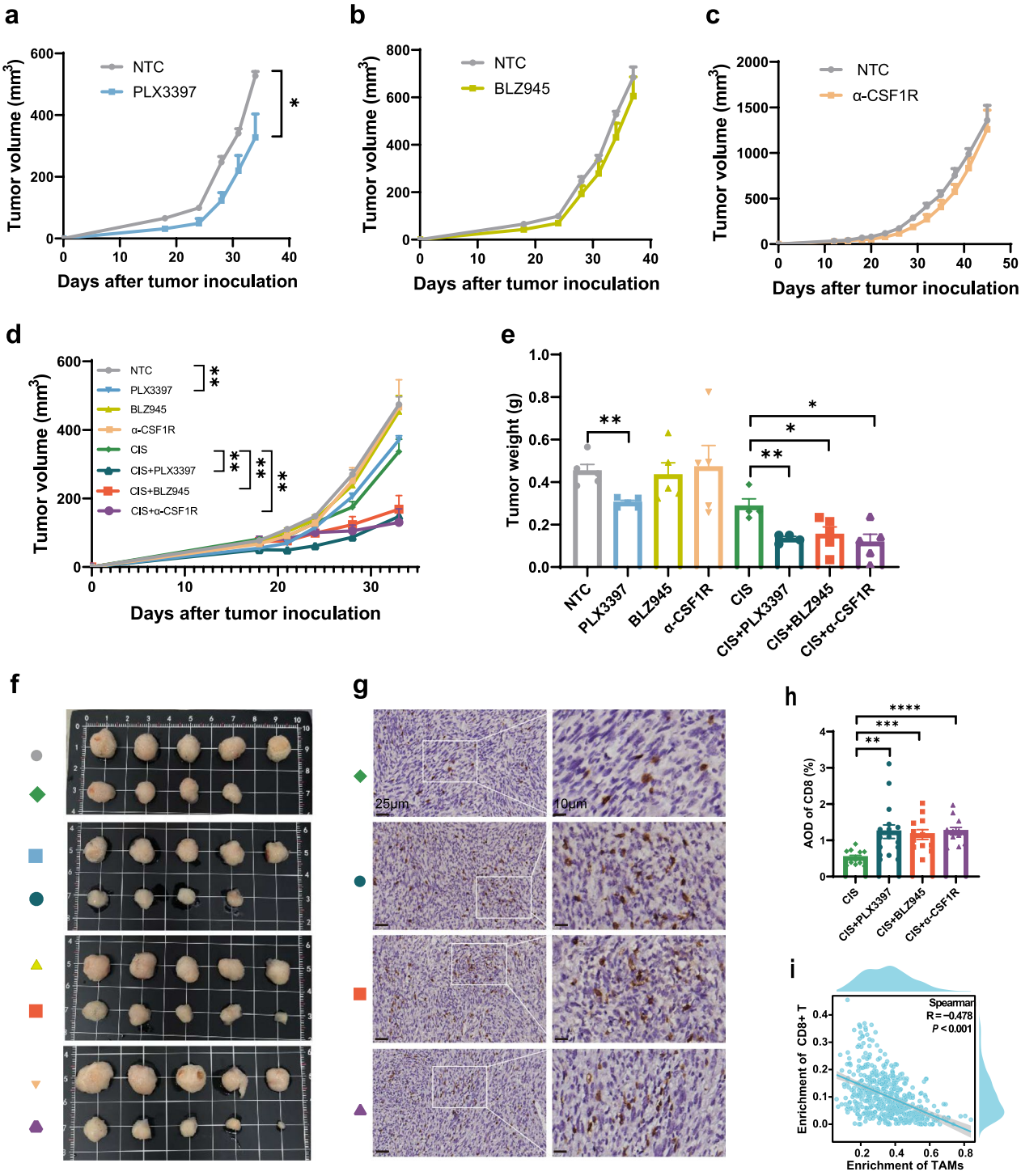


**Fig. 5** (See legend on previous page.)

TAMs and M2 macrophages. In a pancreatic ductal adenocarcinoma (PDAC) mouse model, CSF1R blockade reprogrammed macrophages, enhancing antigen presentation and T cell responses, although it also upregulated immune checkpoints such as PD-L1 [40]. Similarly, we observed upregulation of PD-L1 after CSF1R inhibition (data not shown). In addition to depleting TAMs, CSF1R inhibitors also resulted in increased $CD8^+$ T cells infiltration within the TME. Jonathan B. Mitchem's study showed that CSF1R

inhibition targeting TAMs reduced pancreatic tumor-initiating cells (TICs), increased tumor-infiltrating lymphocytes (TILs), and enhanced gemcitabine efficacy in vivo [23]. Strachan, D.C. found that CSF1R inhibition not only reduced TAMs turnover but also significantly increased $CD8^+$ T cells infiltration in cervical and breast cancers [57]. Our in vivo experiments showed a significant increase in $CD8^+$ T cells infiltration with combination therapy. We propose that CSF1R inhibitors deplete TAMs and enhance $CD8^+$ T cells infiltration by reversing immune suppression. TAMs, particularly M2-type, promote T cell exhaustion through the secretion of immunosuppressive factors like IL-10 [58, 59]. Additionally, TAMs play a crucial role in antigen presentation through receptors such as CD86 and MHC II, which are essential for activating $CD8^+$ T cells [60]. Our in vitro data show that CSF1R inhibitors reduce IL-10 secretion, alter CD86 and MHC II expression, and enhance TAM-mediated phagocytosis of tumor cells. However, further research is needed to clarify the specific relationship between TAMs and $CD8^+$ T cells.

PLX3397 is a competitive CSF-1R inhibitor that blocks signaling, inhibits macrophage proliferation, and promotes TAMs polarization towards the pro-inflammatory M1 phenotype, delaying tumor growth in a hepatocellular carcinoma mouse model [61]. However, a study by Shi et al. suggested that PLX3397 enhances the immunosuppressive TME primarily by reducing the number of TAMs, rather than altering their polarization. [62]. In our in vitro experiments, PLX3397 downregulated CD206, upregulated CD86, and promoted M1 polarization in TAMs, enhancing apoptosis and phagocytosis. However, it also reduced MHC II expression, potentially impairing antigen presentation. BLZ945, another highly selective CSF1R inhibitor, suppresses TAMs activity and proliferation while reprogramming their immunosuppressive properties. Magkouta et al. demonstrated that BLZ945 effectively inhibited tumor progression, reduced TAMs infiltration, and promoted M1 polarization in a mesothelioma mouse model [63]. In our studies, BLZ945 downregulated CD206, enhanced TAM phagocytosis and apoptosis, but had a weaker effect on CD86 and MHC II. However, it showed no significant tumor growth inhibition when used alone in vivo. Additionally, A murine IgG2a monoclonal antibody targeting CSF-1R effectively depleted macrophages in vivo but, like BLZ945, did not significantly suppress tumor growth. In contrast, PLX3397 exhibited the strongest anti-tumor efficacy in our HNSCC mouse model, possibly due to its inhibition of other kinases, such as KIT and FLT3 [64], The varying efficacies of these CSF1R inhibitors likely stem from differences in how they modulate CSF1R signaling and other molecular targets, suggesting that clinical selection should be tailored to specific pathological conditions and therapeutic objectives.

In summary, the impact of CSF1R-targeted TAMs modulation is likely influenced by tumor type, subtype, progression, and individual patient differences. Moreover, different CSF1R inhibitors may regulate TAMs functions through distinct mechanisms, affecting antitumor immune responses. Clinical strategies should therefore be personalized to achieve the most effective treatment outcomes. While CSF1R inhibitors alone did not significantly inhibit tumor growth, their combination with cisplatin notably enhanced antitumor efficacy, suggesting a synergistic interaction, overcoming the limitations of monotherapy. These findings provide valuable insights into TAMs-targeting strategies in HNSCC and underscore the potential of combining CSF1R inhibitors with other therapies to optimize treatment regimens and improve patient outcomes.

**Abbreviations**

| | |
|---|---|
| TAMs | Tumor-Associated Macrophages |
| TME | Tumor Microenvironment |
| HNSCC | Head and Neck Squamous Cell |
| CSF1R | Colony Stimulating Factor 1 Receptor. |
| OS | Overall Survival |
| DFS | Disease-Free Survival |
| HPV | Human Papillomavirus |
| EBV | Epstein-Barr virus |
| NCCN | National Comprehensive Cancer Network |
| EGFR | Epidermal Growth Factor Receptor |
| TCGA | The Cancer Genome Atlas |
| GEO | Gene Expression Omnibus |
| GO | Gene Ontology |
| GSEA | Gene Set Enrichment Analysis |
| OSCC | Oral Squamous Cell Carcinoma |
| ATCC | American Type Culture Collection |
| FBS | Fetal Bovine Serum |
| BMDMs | Bone Marrow-Derived Macrophages |
| TCS | Tumor Cell Supernatant |
| DCs | Dendritic Cells |

## Supplementary Information

The online version contains supplementary material available at https://doi.org/10.1186/s12967-024-06036-3.

Supplementary material 1: Supplementary Figure 1. Survival analysis of HNSCC patients based on macrophage infiltration subtypes.Patients in the TCGA-HNSCC cohort were stratified into high and low infiltration groups for M0, M1, and M2macrophages based on the minimum *p*-value approach. Kaplan-Meier survival curves were generated, and survival differences were assessed using the log-rank test, n = 519.

Supplementary material 2: Supplementary Figure 2. Characterization of macrophage subpopulations using flow cytometry. Flow cytometric characterization of bone marrow-derived macrophages, classical LPS-induced M1 macrophages, IL-4-induced M2 macrophages, and TAMs stimulated with MTCQ1 tumor cell supernatantusing specific markers

Supplementary material 3: Supplementary Figure 3. IHC analysis of TAMs and macrophage subtype infiltration in HNSCC tissues. The expression levels of F4/80, CD163, and iNOS were analyzed by immunohistochemistryto

assess TAM and M2 infiltrationand M1 infiltration. *T*-tests were used for statistical analysis. Scale bars = 50 μm, n = 8. *, $p < 0.05$; **, $p < 0.01$; ***, $p < 0.001$.

**Acknowledgements**
This work was supported by project grants from the National Science Foundation of China (81972896 to T.L.), the Guangdong Province Natural Science Foundation (2019A1515010288 to T.L.), the Guangdong Basic and Applied Basic Research Foundation (2021A1515012620 to J.Liao.), the MOE Key Laboratory of Gene Function and Regulation, the National Key Clinical Discipline, and the State Key Laboratory of Oncology in South China.

**Author contributions**
Conceptualization, J.Liao. and K.C.; Investigation, K.C. and X.L., S.D. and Y.G.; Writing—Original Draft, K.C.; Writing—Review & Editing, J.Liao., S.-M.Z., J.Liu. T.L and W.-P.W.; Visualization, K.C. and S.D., X.L and Z.L.; Supervision, J.Liao., and W.-P.W.; Funding Acquisition, J.Liao. and T.L.

**Availability of data and materials**
The authors confirmed that the data supporting the findings of this study are available within the article and/or supplementary materials.

## Declarations

**Consent for publication**
Not applicable.

**Competing interests**
The authors declare that they have no competing interests.

**Author details**
[1]Department of General Surgery of Otorhinolaryngology Head and Neck, The Sixth Affiliated Hospital, Sun Yat-Sen University, No.26, Erheng Road, Yuancun, Tianhe District, Guangzhou 510655, China. [2]Biomedical Innovation Center, The Sixth Affiliated Hospital, Sun Yat-Sen University, No.26, Erheng Road, Yuancun, Tianhe District, Guangzhou 510655, China. [3]GMU-GIBH Joint School of Life Sciences, The Guangdong-Hong Kong-Macau, Joint Laboratory for Cell Fate Regulation and Diseases, Guangzhou Medical University, No.1 Xinzao Road, Xinzao, Panyu District, Guangzhou 511436, China. [4]Department of Thyroid Surgery, Sun Yat-sen Memorial Hospital, Sun Yat-sen University, No.33, Yingfeng Road, Haizhu District, Guangzhou 510120, China. [5]Department of Otolaryngology, The First Affiliated Hospital of Sun Yat-Sen University, No.58, Zhongshan 2nd Road, Yuexiu District, Guangzhou 510080, China.

Received: 12 October 2024 Accepted: 25 December 2024
Published online: 08 January 2025

**References**

1. International Agency for Research on Cancer. https://gco.iarc.fr. Accessed 21 06 2024.
2. Sung H, et al. Global cancer statistics 2020: GLOBOCAN estimates of incidence and mortality worldwide for 36 cancers in 185 countries. CA Cancer J Clin. 2021;71(3):209–49.
3. Hashibe M, et al. Alcohol drinking in never users of tobacco, cigarette smoking in never drinkers, and the risk of head and neck cancer: pooled analysis in the international head and neck cancer epidemiology consortium. J Natl Cancer Inst. 2007;99(10):777–89.
4. Lee YA, et al. Tobacco smoking, alcohol drinking, betel quid chewing, and the risk of head and neck cancer in an East Asian population. Head Neck. 2019;41(1):92–102.
5. Guha N, et al. Betel quid chewing and the risk of oral and oropharyngeal cancers: a meta-analysis with implications for cancer control. Int J Cancer. 2014;135(6):1433–43.
6. de Martel C, et al. Global burden of cancers attributable to infections in 2008: a review and synthetic analysis. Lancet Oncol. 2012;13(6):607–15.
7. Boffetta P, et al. Occupation and larynx and hypopharynx cancer: an international case-control study in France, Italy, Spain, and Switzerland. Cancer Causes Control. 2003;14(3):203–12.
8. Guha N, et al. Oral health and risk of squamous cell carcinoma of the head and neck and esophagus: results of two multicentric case-control studies. Am J Epidemiol. 2007;166(10):1159–73.
9. Pfister DG, et al. Head and neck cancers, version 2.2020, NCCN clinical practice guidelines in oncology. J Natl Compr Canc Netw. 2020;18(7):873–98.
10. Marur S, Forastiere AA. Head and neck squamous cell carcinoma: update on epidemiology, diagnosis, and treatment. Mayo Clin Proc. 2016;91(3):386–96.
11. Brouns E, et al. Malignant transformation of oral leukoplakia in a well-defined cohort of 144 patients. Oral Dis. 2014;20(3):e19-24.
12. Anderson G, et al. An updated review on head and neck cancer treatment with radiation therapy. Cancers. 2021;13(19):4912.
13. Zhang Y, et al. Gemcitabine and cisplatin induction chemotherapy in nasopharyngeal carcinoma. N Engl J Med. 2019;381(12):1124–35.
14. de Castro G, et al. Criteria for eligibility to cisplatin in the curative treatment of head and neck cancer: consensus opinion from a panel of experts. Crit Rev Oncol Hematol. 2018;131:30–4.
15. Schuette A, et al. Predicting hearing loss after radiotherapy and cisplatin chemotherapy in patients with head and neck cancer. JAMA Otolaryngol Head Neck Surg. 2020;146(2):106–12.
16. Saba NF, et al. Targeting the EGFR and immune pathways in squamous cell carcinoma of the head and neck (SCCHN): forging a new alliance. Mol Cancer Ther. 2019;18(11):1909–15.
17. Burtness B, et al. Pembrolizumab alone or with chemotherapy versus cetuximab with chemotherapy for recurrent or metastatic squamous cell carcinoma of the head and neck (KEYNOTE-048): a randomised, open-label, phase 3 study. Lancet. 2019;394(10212):1915–28.
18. Chen Y, et al. Tumor-associated macrophages: an accomplice in solid tumor progression. J Biomed Sci. 2019;26(1):78.
19. Cassetta L, Pollard JW. Targeting macrophages: therapeutic approaches in cancer. Nat Rev Drug Discov. 2018;17(12):887–904.
20. Locati M, Curtale G, Mantovani A. Diversity, mechanisms, and significance of macrophage plasticity. Annu Rev Pathol. 2020;15:123–47.
21. Qian BZ, Pollard JW. Macrophage diversity enhances tumor progression and metastasis. Cell. 2010;141(1):39–51.
22. Gordon SR, et al. PD-1 expression by tumour-associated macrophages inhibits phagocytosis and tumour immunity. Nature. 2017;545(7655):495–9.
23. Mitchem JB, et al. Targeting tumor-infiltrating macrophages decreases tumor-initiating cells, relieves immunosuppression, and improves chemotherapeutic responses. Cancer Res. 2013;73(3):1128–41.
24. Jensen TO, et al. Macrophage markers in serum and tumor have prognostic impact in American joint committee on cancer stage I/II melanoma. J Clin Oncol. 2009;27(20):3330–7.
25. Steidl C, et al. Tumor-associated macrophages and survival in classic Hodgkin's lymphoma. N Engl J Med. 2010;362(10):875–85.
26. Forssell J, et al. High macrophage infiltration along the tumor front correlates with improved survival in colon cancer. Clin Cancer Res. 2007;13(5):1472–9.
27. Donadon M, et al. Macrophage morphology correlates with single-cell diversity and prognosis in colorectal liver metastasis. J Exp Med. 2020.
28. Bejarano L, Jordao MJC, Joyce JA. Therapeutic targeting of the tumor microenvironment. Cancer Discov. 2021;11(4):933–59.
29. Wu J, et al. SPP1(+) TAM subpopulations in tumor microenvironment promote intravasation and metastasis of head and neck squamous cell carcinoma. Cancer Gene Ther. 2024;31(2):311–21.
30. Xu L, et al. ANXA3-rich exosomes derived from tumor-associated macrophages regulate ferroptosis and lymphatic metastasis of laryngeal squamous cell carcinoma. Cancer Immunol Res. 2024;12(5):614–30.
31. Mok S, et al. Inhibition of CSF-1 receptor improves the antitumor efficacy of adoptive cell transfer immunotherapy. Cancer Res. 2014;74(1):153–61.
32. Chitu V, Stanley ER. Colony-stimulating factor-1 in immunity and inflammation. Curr Opin Immunol. 2006;18(1):39–48.
33. Pixley FJ, Stanley ER. CSF-1 regulation of the wandering macrophage: complexity in action. Trends Cell Biol. 2004;14(11):628–38.

34. Ries CH, et al. Targeting tumor-associated macrophages with anti-CSF-1R antibody reveals a strategy for cancer therapy. Cancer Cell. 2014;25(6):846–59.
35. Paulus P, et al. Colony-stimulating factor-1 antibody reverses chemoresistance in human MCF-7 breast cancer xenografts. Cancer Res. 2006;66(8):4349–56.
36. DeNardo DG, et al. Leukocyte complexity predicts breast cancer survival and functionally regulates response to chemotherapy. Cancer Discov. 2011;1(1):54–67.
37. Salvagno C, et al. Therapeutic targeting of macrophages enhances chemotherapy efficacy by unleashing type I interferon response. Nat Cell Biol. 2019;21(4):511–21.
38. Zhu M, et al. Silence of a dependence receptor CSF1R in colorectal cancer cells activates tumor-associated macrophages. J Immunother Cancer. 2022;10(12):e005610.
39. Gomez-Roca CA, et al. Phase I study of emactuzumab single agent or in combination with paclitaxel in patients with advanced/metastatic solid tumors reveals depletion of immunosuppressive M2-like macrophages. Ann Oncol. 2019;30(8):1381–92.
40. Zhu Y, et al. CSF1/CSF1R blockade reprograms tumor-infiltrating macrophages and improves response to T-cell checkpoint immunotherapy in pancreatic cancer models. Cancer Res. 2014;74(18):5057–69.
41. Rao R, et al. Glioblastoma genetic drivers dictate the function of tumor-associated macrophages/microglia and responses to CSF1R inhibition. Neuro Oncol. 2022;24(4):584–97.
42. Camp RL, Dolled-Filhart M, Rimm DL. X-tile: a new bio-informatics tool for biomarker assessment and outcome-based cut-point optimization. Clin Cancer Res. 2004;10(21):7252–9.
43. Quah HS, et al. Single cell analysis in head and neck cancer reveals potential immune evasion mechanisms during early metastasis. Nat Commun. 2023;14(1):1680.
44. Liu J, et al. FAP is a prognostic marker, but not a viable therapeutic target for clinical translation in HNSCC. Cell Oncol (Dordr). 2024;47(2):623–38.
45. Fujiwara T, et al. CSF1/CSF1R signaling inhibitor pexidartinib (PLX3397) reprograms tumor-associated macrophages and stimulates T-cell infiltration in the sarcoma microenvironment. Mol Cancer Ther. 2021;20(8):1388–99.
46. Wang Y, et al. Early posttraumatic CSF1R inhibition via PLX3397 leads to time- and sex-dependent effects on inflammation and neuronal maintenance after traumatic brain injury in mice. Brain Behav Immun. 2022;106:49–66.
47. Tap WD, et al. Structure-Guided Blockade of CSF1R Kinase in tenosynovial giant-cell tumor. N Engl J Med. 2015;373(5):428–37.
48. Tap WD, et al. Pexidartinib versus placebo for advanced tenosynovial giant cell tumour (ENLIVEN): a randomised phase 3 trial. Lancet. 2019;394(10197):478–87.
49. Klemm F, et al. Compensatory CSF2-driven macrophage activation promotes adaptive resistance to CSF1R inhibition in breast-to-brain metastasis. Nat Cancer. 2021;2(10):1086–101.
50. Hu Y, et al. Tumor-associated macrophages correlate with the clinicopathological features and poor outcomes via inducing epithelial to mesenchymal transition in oral squamous cell carcinoma. J Exp Clin Cancer Res. 2016;35:12.
51. Balermpas P, et al. Head and neck cancer relapse after chemoradiotherapy correlates with CD163+ macrophages in primary tumour and CD11b+ myeloid cells in recurrences. Br J Cancer. 2014;111(8):1509–18.
52. Marcus B, et al. Prognostic factors in oral cavity and oropharyngeal squamous cell carcinoma. Cancer. 2004;101(12):2779–87.
53. Pyonteck SM, et al. CSF-1R inhibition alters macrophage polarization and blocks glioma progression. Nat Med. 2013;19(10):1264–72.
54. Singh S, et al. Chemotherapy coupled to macrophage inhibition induces T-cell and B-cell infiltration and durable regression in triple-negative breast cancer. Cancer Res. 2022;82(12):2281–97.
55. Butowski N, et al. Orally administered colony stimulating factor 1 receptor inhibitor PLX3397 in recurrent glioblastoma: an ivy foundation early phase clinical trials consortium phase II study. Neuro Oncol. 2016;18(4):557–64.
56. Xu J, et al. CSF1R signaling blockade stanches tumor-infiltrating myeloid cells and improves the efficacy of radiotherapy in prostate cancer. Cancer Res. 2013;73(9):2782–94.
57. Strachan DC, et al. CSF1R inhibition delays cervical and mammary tumor growth in murine models by attenuating the turnover of tumor-associated macrophages and enhancing infiltration by CD8(+) T cells. Oncoimmunology. 2013;2(12): e26968.
58. Wei YT, et al. Thymosin alpha-1 reverses M2 polarization of tumor-associated macrophages during efferocytosis. Cancer Res. 2022;82(10):1991–2002.
59. Kerzel T, et al. In vivo macrophage engineering reshapes the tumor microenvironment leading to eradication of liver metastases. Cancer Cell. 2023;41(11):1892-1910 e10.
60. Ma S, et al. YTHDF2 orchestrates tumor-associated macrophage reprogramming and controls antitumor immunity through CD8(+) T cells. Nat Immunol. 2023;24(2):255–66.
61. Ao JY, et al. Colony-stimulating factor 1 receptor blockade inhibits tumor growth by altering the polarization of tumor-associated macrophages in hepatocellular carcinoma. Mol Cancer Ther. 2017;16(8):1544–54.
62. Shi G, et al. Modulating the tumor microenvironment via oncolytic viruses and CSF-1R inhibition synergistically enhances anti-PD-1 immunotherapy. Mol Ther. 2019;27(1):244–60.
63. Magkouta SF, et al. CSF1/CSF1R axis blockade limits mesothelioma and enhances efficiency of anti-PDL1 immunotherapy. Cancers (Basel). 2021;13(11):2546.
64. Patwardhan PP, et al. Sustained inhibition of receptor tyrosine kinases and macrophage depletion by PLX3397 and rapamycin as a potential new approach for the treatment of MPNSTs. Clin Cancer Res. 2014;20(12):3146–58.


## Publisher's Note